DOI: 10.1002/cbic.200700509

Multifunctional Mesoporous Silica Nanoparticles for Intracellular Labeling and Animal Magnetic Resonance Imaging Studies

Si-Han Wu,[a] Yu-Shen Lin,[a] Yann Hung,[a] Yi-Hsin Chou,[b] Yi-Hua Hsu,[b] Chen Chang,*[b] and Chung-Yuan Mou*[a]

The unique properties of mesoporous silica nanoparticles (MSNs), such as high surface areas, uniform pore size, easy modification, and biocompatibility, make them highly suitable for biological applications.[1–2] In previous reports, MSNs have been demonstrated to function as cell markers[3–6] and as gene transfection[7–8] and drug delivery agents.[9–10] Although these cell-level studies are attractive, some important issues, such as the cellular uptake efficiency, toxicity, and circulation behavior of MSNs in living animals, still have to be addressed for further practical animal-level applications.

Superparamagnetic nanoparticles (i.e., magnetite) with diameters of less than 20 nm exhibit effective magnetic resonance imaging (MRI) contrast enhancement behavior. Because MRI is a noninvasive imaging method, it is a powerful tool with which to track the migration of cells and to investigate the distribution of nanoparticles in the living body. The main drawbacks of the MRI technique, however, are low sensitivity and resolution, which make it unable to provide detailed biological information.

In previous reports, magnetic–optical bifunctional nanoparticles have been fabricated for imaging applications. However, they are nonporous hybrid magnetic composites.[11–12] To offset the shortcomings and to expand the bioimaging/delivery applications, simultaneous attachment of a fluorescent probe (subcellular imaging) and a MRI probe (noninvasive imaging) to MSN is an important task. Recently, we adopted a strategy involving the simultaneous fusion of amorphous silica shells of Fe_3O_4@SiO_2 nanoparticles with MSNs that are attached to fluorescein isothiocyanate (FITC).[13] These nanoparticles with multifunctionalities—fluorescent, magnetic, and porous (Mag-Dye@MSNs)—can simultaneously serve as bimodal imaging probes and drug reservoirs. Thus, we believe that Mag-Dye@MSNs would be a suitable material with which to study the cellular uptake efficiency, toxicity, and accumulative behavior of MSNs in living animals. To the best of our knowledge, this is the first report of direct injection of mesoporous silica nanoparticles (MSNs) into mice and of in vivo visualization of the localization of MSNs by MRI.

Mag-Dye@MSNs were synthesized according to the method we previously developed[13] (the detailed synthetic method is described in the Experimental Section). A transmission electron microscopy (TEM) image of the Mag-Dye@MSNs (Figure 1) shows that mostly one Fe_3O_4@SiO_2 nanoparticle was attached to one MSN. The inset figure further confirms that Mag-Dye@MSNs have a well ordered 2D hexagonal structure, which is consistent with the X-ray diffraction (XRD) spectrum. With regard to the physical properties of Mag-Dye@MSNs, their surface area, pore volume, and pore size are 839 $m^2 g^{-1}$, 0.67 $cm^3 g^{-1}$, and 2.5 nm, respectively. Water-suspended Mag-Dye@MSNs exhibit the typical fluorescein emission (λ_{em} = 515 nm). The T_2 relaxivity (r_2, the efficiency of a contrast agent) of the Mag-Dye@MSNs was determined to be 153 $mM^{-1} s^{-1}$ at 40 °C. The iron content (1 wt%) of the Mag-Dye@MSNs was determined by inductively coupled plasma-atomic emission spectroscopy (ICP-AES). All the data described above show that Mag-Dye@MSNs simultaneously possess MRI enhancing, luminescent, and porous properties.

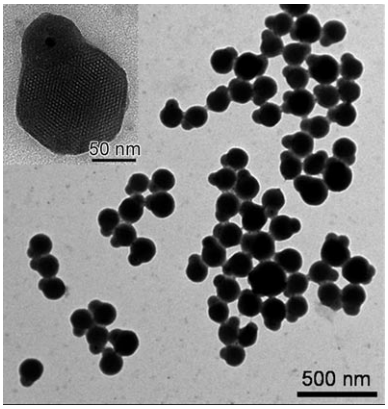

Figure 1. TEM image of Mag-Dye@MSNs. The high-magnification TEM image (inset) shows the well ordered mesoporous and magnetic parts.

To evaluate the in vitro cytotoxicity of Mag-Dye@MSNs, cell viability was examined by MTT assay. As shown in Figure 2A, cell proliferation was not hindered by the presence of Mag-Dye@MSNs. To examine the cell-labeling efficiency, both rat bone marrow stromal cells (rMSCs) and NIH 3T3 fibroblast cells were incubated with various concentrations (20, 40, 60, 80 $\mu g mL^{-1}$) of Mag-Dye@MSNs for 1 h. The flow cytometry results showed that when the Mag-Dye@MSNs (40 $\mu g mL^{-1}$) were incubated with the cells for 1 h, more than 90% of rMSC and NIH 3T3 cells were labeled (Figure 2B). This indicated cells can

[a] S.-H. Wu, Y.-S. Lin, Dr. Y. Hung, Prof. C.-Y. Mou
Department of Chemistry, National Taiwan University
Taipei 106 (Taiwan)
Fax: (+886) 2-23660954
E-mail: cymou@ntu.edu.tw

[b] Y.-H. Chou, Y.-H. Hsu, Dr. C. Chang
Institute of Biomedical Sciences, Academia Sinica
Taipei 115 (Taiwan)
Fax: (+886) 2-27887641
ica.edu.tw
E-mail: bmcchen@ibms.sin

Supporting information for this article is available on the WWW under http://www.chembiochem.org or from the author.

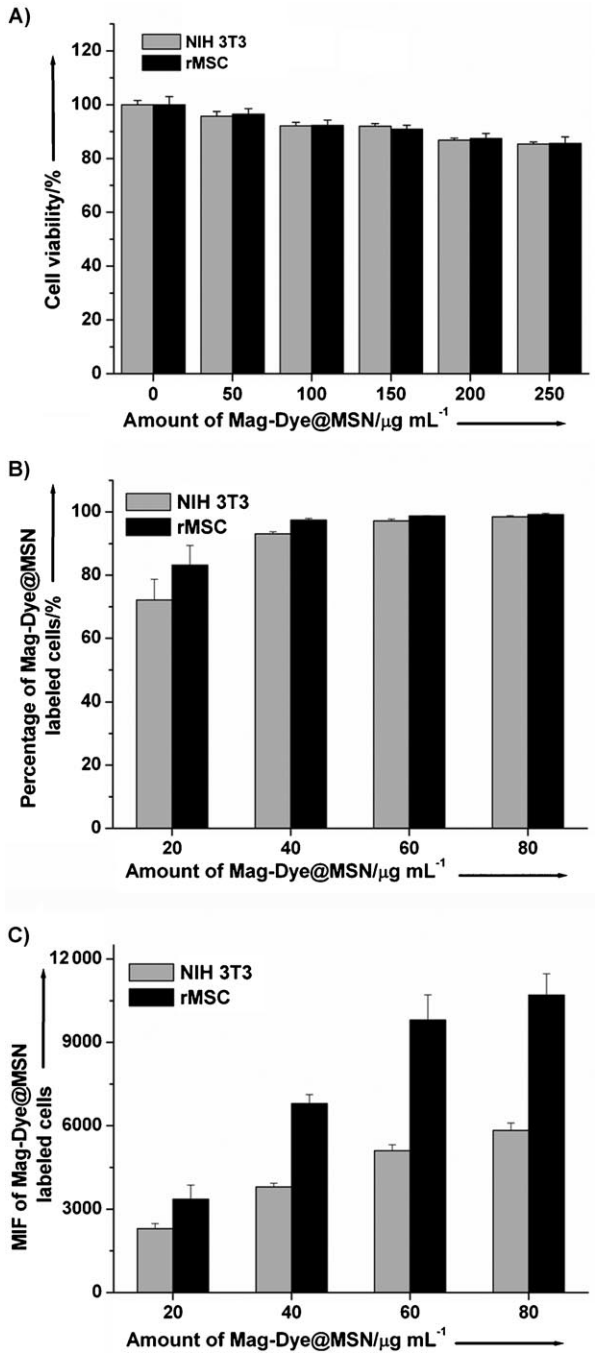

Figure 2. A) The effect of Mag-Dye@MSNs on cell proliferation. Flow cytometry analyses of: B) the percentage and C) mean fluorescence intensity (MFI) of Mag-Dye@MSN-labeled cells.

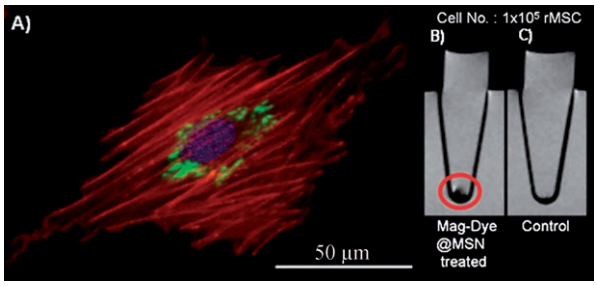

Figure 3. A) Merged confocal image of rMSCs that had been allowed to grow in regular growth medium, overnight, after 1 h of incubation with Mag-Dye@MSNs. The cytoskeleton was stained with rhodamine phalloidin (red) and the cell nucleus with DAPI (blue). The T_2-weighted MR images of: B) labeled rMSCs (1×10^5) after treatment with Mag-Dye@MSNs (80 μg mL^{-1}) for 1 h, and C) unlabeled rMSCs (1×10^5) without Mag-Dye@MSNs.

be labeled efficiently within a short incubation time with use of a relatively low dose of Mag-Dye@MSNs. Interestingly, the histograms of mean value of fluorescence intensity (MFI) showed that the level of Mag-Dye@MSNs in rMSC cells was higher than in NIH 3T3 cells (Figure 2C). This result is encouraging for stem cell tracking and therapy.

By using confocal imaging rMSCs that had been allowed to grow in regular growth medium, overnight, after incubation with Mag-Dye@MSNs for 1 h, were examined (Figure 3A). Results showed that the green-emitting Mag-Dye@MSN nanoparticles had indeed internalized into the rMSCs. An interesting phenomenon is that the Mag-Dye@MSNs did not enter the nucleus, but instead surrounded it. Moreover, in vitro T_2-weighted MR images showed MR contrast effects with labeled rMSCs when compared with unlabeled rMSCs. A significantly negative signal enhancement was caused by Mag-Dye@MSNs in treated rMSCs (Figure 3B), whereas no MR image contrast was observed with unlabeled cells (Figure 3C). This result means that 1×10^5 labeled rMSCs could be detected in vitro in a 4.7 T MR scanner and could be used as a base number for in vivo rMSC tracking experiments.

The in vivo contrast enhancing effect of Mag-Dye@MSNs was evaluated in anesthetized mice ($N=3$) with a 7 T MRI system (Bruker Pharmascan). Typically, Mag-Dye@MSNs suspended in deionized water were administrated to mice through eye vein injection at a dose of 5 mg Fe per kg (body weight). Figure 4 shows T_2-weighted MR images of mouse liver, kidneys, and spleen before and after administration of Mag-Dye@MSNs. As time went on, the Mag-Dye@MSNs tended to accumulate more in liver and spleen tissue than in kidney; in fact they appeared to have cleared kidney after 2 h. This phenomenon is similar to literature reports[14–16] in which small superparamagnetic iron oxides (SPIOs, 30–1000 nm) were used for reticulo-endothelial system (RES) specific imaging of liver and spleen, in which the biodistribution is mainly determined by factors such as particle size,[17–18] surface coating,[19–20] and charge.[21] The time-dependent darkening of the MR images in liver, spleen, and kidneys (including renal pelvis, renal medulla, and renal cortex) after administration of Mag-Dye@MSNs was also confirmed quantitatively (Figure 5A). This showed that the recover time of signal-to-noise ratio (SNR) in kidneys was notably shorter than that in liver/spleen, indicating that most Mag-Dye@MSNs were trapped by the RES organs. In addition, using a fluorescence microscope, we clearly observed green spots in histology slides taken from perfused or nonperfused mice sacrificed 30 min after administration of the green-emitting Mag-Dye@MSNs. By these means, we could visualize the fluorescent foci clearly in the liver and spleen (Figure 6), but not in the kidneys. This is due to the lower concentration of Mag-Dye@MSNs in kidneys. We noticed that the fluorescent foci in mice that were not perfused were stronger than in perfused ones; this

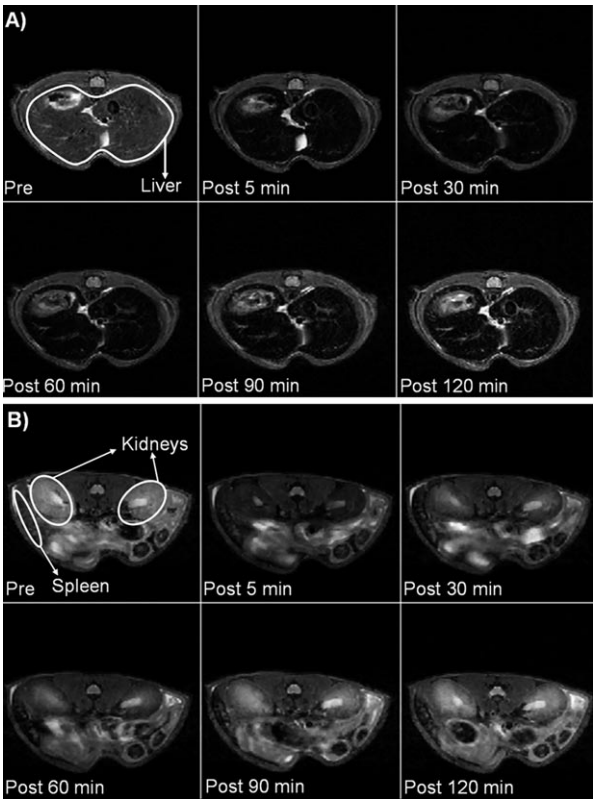

Figure 4. In vivo T_2-weighted MR images before (pre) and after (post) administration of 5 mg Fe per kg body weight of Mag-Dye@MSNs (post 5, 30, 60, 90, and 120 min). A) Liver, and B) kidneys/spleen images showed time-dependent darkening in MR images.

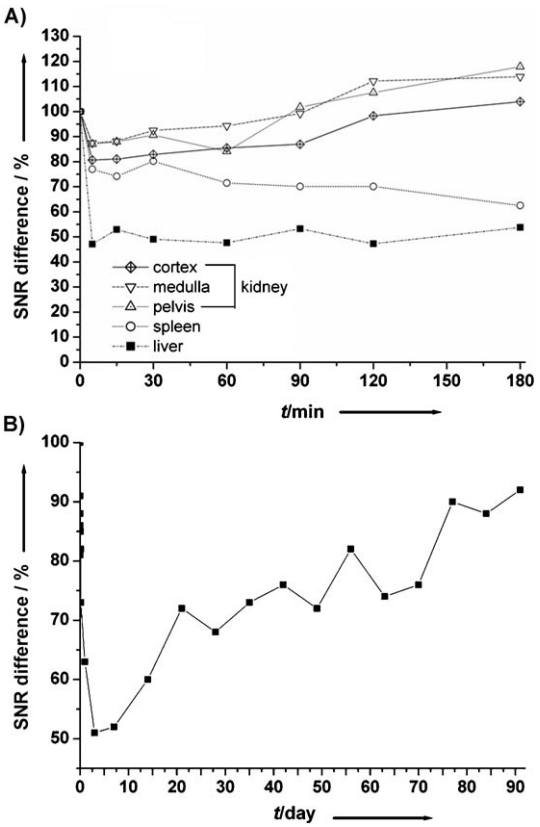

Figure 5. A) Time-dependent changes in the SNR difference in the liver, spleen, renal cortex, renal medullar, and renal pelvis after administration of Mag-Dye@MSNs (5 mg Fe per kg body weight; number of mice, $N = 3$). B) Long-term SNR difference in the liver after administration of Mag-Dye@MSNs (2 mg Fe per kg body weight).

implies that the nanoparticles were still in the blood vessel 30 min after administration. Perl's Prussian blue stain (iron stain) and immunochemical staining showed that only a few Mag-Dye@MSNs were taken up by macrophages at the time point of 30 min after administration (data not shown). We believe that Mag-Dye@MSNs darken liver/spleen T_2-weighted MR images predominantly through a vascular mechanism in the early stages, and that signal darkening was due to particle accumulation within the RES in the late stages.

As a long-term MRI tracking study, we monitored the liver for three months. The result revealed that the SNR recovered after 90 days (Figure 5 B). The slow recovery meant that Mag-Dye@MSNs were resistant to decomposition and not easily excreted from the body. We are continuing to study the final fate of the MSNs. We believe that these Mag-Dye@MSNs could be a potential candidate for long-term liver/spleen MRI monitoring and targeted drug delivery.

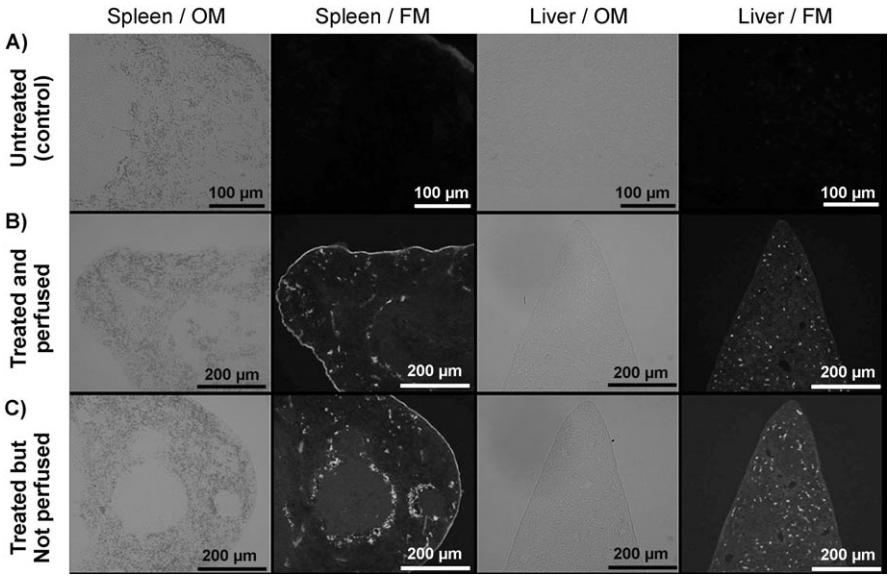

Figure 6. Histological sections of various tissue organs removed 30 min after administration of Mag-Dye@MSNs (5 mg Fe per kg body weight) and examined under an optical microscope (OM) and a fluorescence microscope (FM). A) Mag-Dye@MSNs untreated (control), B) treated and perfused, C) treated but not perfused.

For ultimate diagnostic purposes, toxicity is a main concern for all contrast agents injected intravenously. We note that the mice used for MRI studies showed no obvious abnormalities after recovering from anesthesia, even though extensive toxicity studies (such as the LD_{50}, pharmacokinetics, and biodegradation studies) are currently not completely investigated. Preliminary results show that no abnormal clinical signs were observed after administration of a dose of 2 mg Fe per kg body weight ($N=3$), and that no statistical differences in the body weight changes between controls and Mag-Dye@MSN-treated mice were detected during a four-week study period (Figure S1). All mice survived until they were sacrificed.

The utility of multifunctional Mag-Dye@MSNs resides in their ability to combine organic/inorganic and diagnostic/therapeutic components within the nanoscale. We have demonstrated the advantage of multifunctional nanoparticles in histology samples, in which fluorescence can be used to detect the presence of nanoparticles directly in the animal without further staining. The reported experiments are crucial to the in vivo application of Mag-Dye@MSNs: they provide baseline information for the use of mesoporous silica nanoparticles as diagnostic reagents and therapeutic drug carriers.

Experimental Section

Synthesis of Mag-Dye@MSNs: Mag-Dye@MSNs were synthesized by previously reported procedures.[13] Firstly, size-controlled and monodispersed superparamagnetic nanocrystals (Fe_3O_4) were synthesized by the thermal decomposition method.[22] Then, water-suspended Fe_3O_4@SiO_2 nanoparticles were synthesized by a water-in-oil reverse micelle method.[23] Finally, multifunctional mesoporous silica nanoparticles (Mag-Dye@MSNs) were formed by addition of organic dyes (FITC) and Fe_3O_4@SiO_2 to an ammonia solution containing dilute TEOS and low surfactant concentration. The as-synthesized Mag-Dye@MSNs were extracted by a fast and efficient ion-exchange method,[24] and were then collected by centrifugation and redispersed in water. Mag-Dye@MSNs were characterized by using various techniques, including XRD (PANalytical's X'Pert PRO X-ray diffractometer), TEM (JEOL JEM1230), ICP-AES (Kontron S-35), N_2 adsorption-desorption isotherms (Micromeritics ASAP 2010), photoluminescence spectroscopy (Hitachi F-4500), and T_2 relaxation time measurements (0.47 T, Bruker Minispec).

Cell culture: rMSCs (rat bone marrow stromal cells) were obtained from Dominion Pharmakine and cultured in regular growth medium consisting of DMEM/F12 (GIBCO) supplemented with fetal bovine serum (GIBCO, 20%) and penicillin/streptomycin (GIBCO, 1%). NIH 3T3 fibroblasts (American Type Culture Collection) were cultured in DMEM (GIBCO) containing fetal bovine serum (GIBCO, 10%) and penicillin/streptomycin (GIBCO, 1%) in a humidified atmosphere with CO_2 (5%) at 37 °C.

Cell proliferation assay: Cells (1×10^5 per well) were seeded in 24-well plates for proliferation assays. After incubation with different amounts of Mag-Dye@MSN suspension in serum-free medium for 1 h, cells were allowed to grow in regular growth medium for 24 h, followed by incubation with fresh serum-free medium containing 3-(4,5-dimethylthiazol-2-yl)-2,5-diphenyl-tetrazolium bromide (0.5 mg mL^{-1}) for 4 h at 37 °C for proliferation assay. The dark blue formazan dye generated by the live cells was proportional to the number of live cells, and the absorbance at 570 nm was measured with a microplate reader (Bio-Rad, model 680). Cell numbers were determined from a standard plot of known cell numbers versus the corresponding optical density.

Cellular uptake assays: Different types of cells (rMSC, NIH 3T3) were seeded at 1.2×10^5 cells per well in 6-well plates and allowed to attach for 24 h. To determine the nanoparticle uptake and the extent of loading, the cells were incubated with a planned amount of nanoparticles suspended in serum-free medium for an intended incubation time. Treated cells were then washed three times with phosphate-buffered saline (PBS: 137 mM NaCl, 2.68 mM KCl, 10 mM Na_2HPO_4, 1.76 mM KH_2PO_4, pH 7.4), and then harvested by trypsinization. The green emitting fluorescein dye (excited at 488 nm with an argon laser and detected at a wavelength in the 510 to 540 nm range) incorporated in the nanoparticles served as a marker for quantitative determination of their cellular uptake, which was analyzed by flow cytometry (BD FACSAria Cell-Sorting System) with CellQuest Pro software (BD, Mississauga, CA, USA).

Magnetic resonance imaging and data analysis: In vitro T_2-weighted MR images were acquired with a 4.7 T MR scanner (Bruker Biospec). To prepare the cells for MRI, 1×10^5 rMSCs were incubated with Mag-Dye@MSN (80 μg mL^{-1}). After 1 h incubation, the cells were washed twice with PBS solution, trypsinized, and collected in 0.5 mL Eppendorf tubes by centrifugation. After centrifugation, the Eppendorf tubes were placed in a water bath and were then scanned in a 4.7 T MR scanner (Bruker Biospec), repetition time (TR)/echo time (TE) = 4000 ms/80 ms, field of view (FOV) = 6 cm, number of excitations (NEX) = 4, spectral width (SW) = 41 666.7 Hz, slice thickness (Slth) = 2.0 mm, matrix = 256×256. In vivo T_2-weighted MR images were acquired with a 7 T MR scanner (Bruker Pharmascan) before and at different times after the injection of Mag-Dye@MSN nanoparticles. Typically, nanoparticles suspended in deionized water (0.1 mL) were administrated to Institute of Cancer Research (ICR) mice (5 to 8 weeks of age, body mass ≈25 g, ICR mouse) through eye vein injection at a dose of 5 mg Fe per kg body weight. The measurement parameters were as follows: TR/TE = 4000 ms/40 ms, FOV = 3 cm, NEX = 4, SW = 57 471.3 Hz, Slth = 1.0 mm, matrix = 256×128, and temperature = 37 °C. For T_2-weighted images, the signal intensities (SIs) and signal-to-noise ratio ($SNR = SI_x/SI_{noise}$) were measured for liver, spleen, and kidneys. The percentage of SNR change for pre-injection versus postinjection imaging was calculated according to the following formula:

$$\%\ \text{SNR difference} = 100 \times ([SNR]_{post} - [SNR]_{pre})/[SNR]_{post}$$

Histology: In order to correlate MR signal changes with histological evidence, animals were sacrificed after MRI experiments. If needed, the mice were perfused transcardially with paraformaldehyde (Sigma, 4%) in PBS (pH 7.4). The kidneys, spleen, and liver were removed, kept in the same fixative overnight at 4 °C, paraffinized, and sectioned at 5 μm. One set of kidney/spleen/liver sections was stained with hematoxylin and eosin for the visualization of the tissue structure. Another set of sections was stained with Perl's Prussian blue staining for the detection of iron particles (data not shown). The stained sections were examined under light microscopy by two well trained experimenters who were blind to the state of the mice under investigation. A third set was examined by fluorescence microscope (Olympus BX51). All animal experiments were approved by the Institutional Animal Care and Utilization Committee at the Academia Sinica, Taipei, Taiwan.

Acknowledgements

This research was supported by a grant from the National Science Council of Taiwan. Technical support from the Functional and Micro-Magnetic Resonance Imaging Center supported by the National Research Program for Genomic Medicine, Taiwan is acknowledged. We thank Yi-Chun Chuang for help with confocal microscopy measurements.

Keywords: cell tracking · imaging agents · magnetic resonance imaging · mesoporous materials · nanoparticles

[1] M. Vallet-Regí, *Chem. Eur. J.* **2006**, *12*, 5934–5943.
[2] I. I. Slowing, B. G. Trewyn, S. Giri, V. S.-Y. Lin, *Adv. Funct. Mater.* **2007**, *17*, 1225–1236.
[3] Y.-S. Lin, C.-P. Tsai, H.-Y. Huang, C.-T. Kuo, Y. Hung, D.-M. Huang, Y.-C. Chen, C.-Y. Mou, *Chem. Mater.* **2005**, *17*, 4570–4573.
[4] D.-M. Huang, Y. Hung, B.-S. Ko, S.-C. Hsu, W.-H. Chen, C.-L. Chien, C.-P. Tsai, C.-T. Kuo, J.-C. Kang, C.-S. Yang, C.-Y. Mou, Y.-C. Chen, *FASEB J.* **2005**, *19*, 2014–2016.
[5] I. I. Slowing, B. G. Trewyn, V. S.-Y. Lin, *J. Am. Chem. Soc.* **2006**, *128*, 14792–14793.
[6] T.-H. Chung, S.-H. Wu, M. Yao, C.-W. Lu, Y.-S. Lin, Y. Hung, C.-Y. Mou, Y.-C. Chen, D.-M. Huang, *Biomaterials* **2007**, *28*, 2959–2966.
[7] D. R. Radu, C.-Y. Lai, K. Jeftinija, E. W. Rowe, S. Jeftinija, V. S.-Y. Lin, *J. Am. Chem. Soc.* **2004**, *126*, 13216–13217.
[8] F. Torney, B. G. Trewyn, V. S.-Y. Lin, K. Wang, *Nat. Nanotechnol.* **2007**, *2*, 295–300.
[9] C.-Y. Lai, B. G. Trewyn, D. M. Jeftinija, K. Jeftinija, S. Xu, S. Jeftinija, V. S.-Y. Lin, *J. Am. Chem. Soc.* **2003**, *125*, 4451–4459.
[10] J. Lu, M. Liong, J. I. Zink, F. Tamanoi, *Small* **2007**, *3*, 1341–1346.
[11] J. Kim, J. E. Lee, J. Lee, Y. Jang, S.-W. Kim, K. An, J. H. Yu, T. Hyeon, *Angew. Chem.* **2006**, *118*, 4907–4911; *Angew. Chem. Int. Ed.* **2006**, *45*, 4789–4793.
[12] T.-J. Yoon, K. N. Yu, E. Kim, J. S. Kim, B. G. Kim, S.-H. Yun, B.-H. Sohn, M.-H. Cho, J.-K. Lee, S. B. Park, *Small* **2006**, *2*, 209–215.
[13] Y.-S. Lin, S.-H. Wu, Y. Hung, Y.-H. Chou, C. Chang, M.-L. Lin, C.-P. Tsai, C.-Y. Mou, *Chem. Mater.* **2006**, *18*, 5170–5172.
[14] J. T. Ferrucci, D. D. Stark, *AJR Am. J. Roentgenol.* **1995**, *155*, 943–950.
[15] R. Weissleder, D. D. Stark, B. L. Engelstad, B. R. Bacon, C. C. Compton, D. L. White, P. Jacobs, J. Lewis, *AJR Am. J. Roentgenol.* **1989**, *152*, 167–173.
[16] J. S. Kim, T.-J Yoon, K. N. Yu, B. G. Kim, S. J. Park, H. W. Kim, K. H. Lee, S. B. Park, J.-K. Lee, M. H. Cho, *Toxicol. Sci.* **2006**, *89*, 338–347.
[17] C. Bremer, T. Allkemper, J. Baermig, P. Reimer, *J. Magn. Reson. Imag.* **1999**, *10*, 461–467.
[18] J. B. Mandeville, J. Moore, D. A. Chesler, L. Garrido, R. Weissleder, R. M. Weisskoff, *Magn. Reson. Med.* **1997**, *37*, 885–890.
[19] D. J. Widder, W. L. Greif, K. J. Widder, R. R. Edelman, T. J. Brady, *AJR Am. J. Roentgenol.* **1987**, *148*, 399–404.
[20] A. Moore, R. Weissleder, A. Bogdanov, Jr., *J. Magn. Reson. Imaging* **1997**, *7*, 1140–1145.
[21] R. Weissleder, A. Bogdanov, E. A. Neuwelt, M. Papisov, *Adv. Drug Delivery Rev.* **1995**, *16*, 321–334.
[22] S. Sun, H. Zeng, *J. Am. Chem. Soc.* **2002**, *124*, 8204–8205.
[23] C.-W. Lu, Y. Hung, J.-K. Hsiao, M. Yao, T.-H. Chung, Y.-S. Lin, S.-H. Wu, S.-C. Hsu, H.-M. Liu, C.-Y. Mou, C.-S. Yang, D.-M. Huang, Y.-C. Chen, *Nano. Lett.* **2007**, *7*, 149–154.
[24] N. Lang, A. Tuel, *Chem. Mater.* **2004**, *16*, 1961–1966.

Received: August 30, 2007
Published online on November 12, 2007

